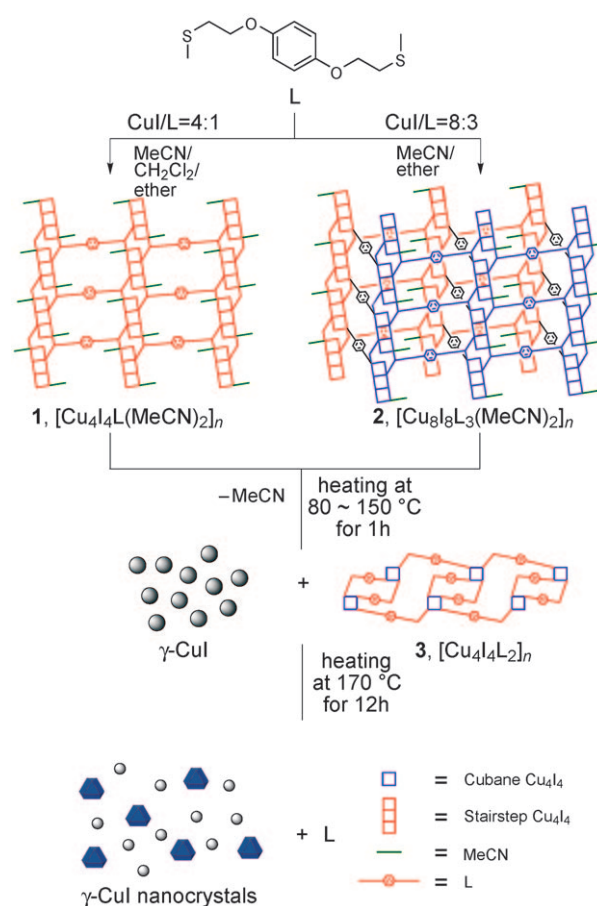


$\gamma$ -CuI Nanocrystals from Self-Assembled Coordination PolymersTae Ho Kim, Hojin Yang, Garam Park, Kang Yeol Lee, and Jineun Kim\*<sup>[a]</sup>

The architectural control of nanocrystals has attracted remarkable attention because of intriguing size-, shape-, and special orientation-dependent properties.<sup>[1–4]</sup> Understanding of the properties of individual nanocrystals will enable us to exploit them, making it possible to design and build novel electronic, magnetic, and photonic devices and other functional materials based on these nanostructures. The utilization of coordination compounds as both precursor and template is one of the versatile ways for the preparation of nanomaterials. There are few reports which utilize coordination polymers to synthesize metal oxides, sulfides, and nanowires.<sup>[5–7]</sup> Despite these advances, it is still a challenge to develop a synthetic approach which can predict the size and shape of the nanomaterials with respect to the reactants. The preparation of CuI has been carried out by several different methods, such as liquid-phase reaction,<sup>[8]</sup> laser deposition,<sup>[9]</sup> vacuum evaporation,<sup>[10]</sup> and solvothermal techniques.<sup>[11,12]</sup> Herein we report the syntheses of two self-assembled Cu<sup>I</sup> coordination polymers **1** and **2**, crystal transformation from **1** and **2** into an intermediate Cu<sup>I</sup> coordination polymer **3** with  $\gamma$ -CuI nanocrystals and 1,4-bis(2-methylthioethoxy)benzene **L** by heating the polymers. We also describe that thermal decomposition of the Cu<sup>I</sup> polymer **3** results in  $\gamma$ -CuI nanocrystals and **L**.

Scheme 1 shows the syntheses of microcrystals of the two copper(I) coordination polymers  $[\text{Cu}_4\text{I}_4\text{L}(\text{MeCN})_2]_n$  (**1**) and  $[\text{Cu}_8\text{I}_8\text{L}_3(\text{MeCN})_2]_n$  (**2**) by the self-assembly of CuI and **L**. Heating both **1** and **2** near 105 °C resulted in  $[\text{Cu}_4\text{I}_4\text{L}_2]_n$  (**3**) and  $\gamma$ -CuI nanocrystals known as a *p*-type semiconductor with a band gap of about 3.1 eV.<sup>[13,14]</sup> The polymer **3** decom-



Scheme 1. Preparation of coordination polymers **1–3** and  $\gamma$ -CuI nanocrystals.

posed upon heating at 170 °C to yield  $\gamma$ -CuI nanocrystals and **L**.

The ligand was prepared by the reaction of hydroquinone and 2-chloroethylmethylsulfane in acetone, using potassium carbonate as a base.<sup>[15]</sup> Slow evaporation yields good-quality crystals for single-crystal X-ray diffraction (SCXRD; Scheme S1 in the Supporting Information; crystal data of **L** are listed in Table S1, and an ORTEP view is shown in Figure S1). The coordination polymer **1** was synthesized by the

[a] Dr. T. H. Kim, H. Yang, G. Park, Dr. K. Y. Lee, Prof. J. Kim  
Department of Chemistry(BK21) and Research Institute of Natural Science  
Gyeongsang National University  
900 Gajwa-dong, Jinju 660-701(South Korea)  
Fax: (+82)55-758-5532  
E-mail: jekim@gnu.ac.kr  
Homepage: <http://inorglab.gnu.ac.kr>

Supporting information for this article is available on the WWW under <http://dx.doi.org/10.1002/asia.200900416>.

self-assembly reaction of stoichiometric amounts of CuI and L (CuI/L=4:1) in a mixture of acetonitrile and dichloromethane at room temperature followed by diffusion of diethyl ether (Figure S2a in the Supporting Information). The polymer **1** was also obtained by using an excess of CuI in acetonitrile instead of using dichloromethane. Without dichloromethane under stoichiometric conditions, polymer **1** was contaminated by a small amount of the polymer **2** (Figure S2b in the Supporting Information).

Pure coordination polymer **2** was synthesized by the self-assembly reaction of stoichiometric amounts of CuI and L (CuI/L=8:3) in acetonitrile at room temperature followed by diffusion of diethyl ether. The use of values between their molar ratios yielded a mixture of the two polymers. Slow diffusion of diethyl ether gave good-quality crystals for SCXRD, while rapid mixing by ultrasonication resulted in microcrystalline powders (Figure S2c in the Supporting Information). The crystals of **1** and **2** grow as block and needle crystals, respectively. The compounds have been characterized by IR, elemental analysis, SCXRD, and powder X-ray diffraction (PXRD) studies (see the Supporting Information).

SCXRD reveals that **1** is a 2D grid network parallel to the crystallographic *a* axis (Figure S3b and Table S3 in the Supporting Information). The network lies in the (011) plane of the unit cell. Each square compartment of the grid (red grid at left-hand side in Scheme 1) is composed of two stairstep Cu<sub>4</sub>I<sub>4</sub> tetramers, two acetonitrile molecules, and two ligands. All copper atoms in the Cu<sub>4</sub>I<sub>4</sub> tetramer have distorted tetrahedral geometries. The inner copper atom (Cu1) in the tetramer is coordinated by three iodide ions and an S donor and the outer copper atom (Cu2) is coordinated by two iodide ions, an S atom, and an acetonitrile molecule, which gives CN stretching bands at 2299 and 2264 cm<sup>-1</sup> in the IR spectrum (Figure S4 in the Supporting Information).

The complex **2** features a 2D supramolecular bilayer network generated by linking two single-layered networks (red and blue layers at right-hand side in Scheme 1; Figure S5b and Table S5 in the Supporting Information) parallel to the *ac* plane. The single layer is similar to that of **1** except that half of the acetonitrile molecules are replaced by the interconnecting ligands (black tilted pillaring ligands in Scheme 1). Coordinated acetonitrile molecules are also bonded to outer copper atoms of the stairstep Cu<sub>4</sub>I<sub>4</sub> tetramers, as evidenced by weaker CN stretching bands at 2306 and 2274 cm<sup>-1</sup> than those of **1** (Figure S4 in the Supporting Information). The purity of the powders **1** and **2** was checked by scanning electron microscopy images and PXRD patterns (Figure S2, S6, and S7 in the Supporting Information).

Thermogravimetric analysis (TGA) and differential thermal analysis (DTA) curves of **1** and **2** are shown in Figure S8 in the Supporting Information. The TGA curves of **1** and **2** indicate that the weight loss begins at 80°C and completes at about 130°C. The DTA curves of **1** and **2** show the first endothermic peaks at about 105°C. This corresponds to

heat absorption owing to the loss of coordinated acetonitrile molecules and transformation from stairstep Cu<sub>4</sub>I<sub>4</sub> polymers to an unknown compound (identified as the cubane Cu<sub>4</sub>I<sub>4</sub> polymer **3**, [Cu<sub>4</sub>I<sub>4</sub>L<sub>2</sub>]<sub>n</sub>) and γ-CuI nanocrystals. The loss of acetonitrile in **1** and **2** changes the ratio of CuI and L and causes the formation of the new compound **3**, and extra CuI becomes γ-CuI nanocrystals. The second endothermic change occurs in the range of 160–190°C. This corresponds to decomplexation to yield the free ligand and γ-CuI nanocrystals. Since Cu–S bonds in the cubane Cu<sub>4</sub>I<sub>4</sub> polymer become labile and the free ligand is liquid at temperatures near 170°C, decomplexation takes place. Probably decomplexed Cu<sub>4</sub>I<sub>4</sub> clusters stick to the seed crystals of γ-CuI and therefore γ-CuI nanocrystals grow. We reported crystal-to-crystal transformation from 1D loop-chain coordination polymers [Cu<sub>2</sub>I<sub>2</sub>(C<sub>12</sub>H<sub>21</sub>NOS<sub>2</sub>)<sub>2</sub>]<sub>n</sub> and [Cu<sub>4</sub>I<sub>4</sub>(C<sub>12</sub>H<sub>21</sub>NOS<sub>2</sub>)<sub>2</sub>]<sub>n</sub> to 2D network coordination polymer [Cu<sub>4</sub>I<sub>4</sub>(C<sub>12</sub>H<sub>21</sub>NOS<sub>2</sub>)<sub>2</sub>]<sub>n</sub>.<sup>[16]</sup> It seems that this crystal transformation can be possible because Cu–S bonds are labile at 180°C. At 170°C, the compounds **1**, **2**, and **3** were completely transformed into γ-CuI nanocrystals and L. The sizes of the γ-CuI nanocrystals depend on heating time. The NMR spectrum of recovered L after heating was the same as that of the free ligand (Figure S9 in the Supporting Information). The second weight loss begins at about 200°C and ends at about 320°C, which corresponds to evaporation of the ligand.

According to the TGA and DTA results, we heated **1** and **2** in the range of 80–170°C and measured the PXRD patterns (Figure 1, and Figure S10 in the Supporting Information). The same PXRD patterns were obtained from heated

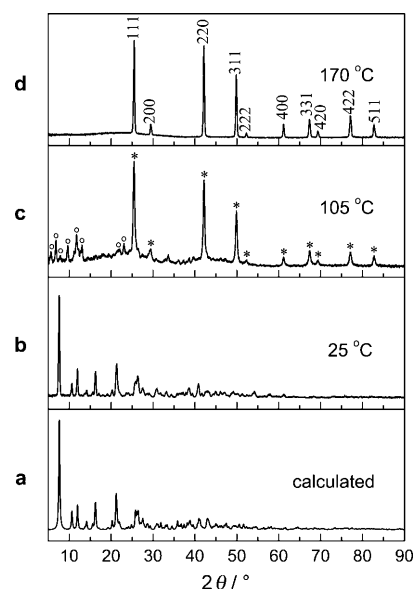


Figure 1. PXRD patterns of **1** before and after heating at different temperatures. a) Calculated PXRD pattern of **1** with the SCXRD data. b) PXRD pattern of **1**. c) PXRD pattern after heating **1** at 105°C. Open circles and asterisks are assigned to **3** and γ-CuI nanocrystals, respectively. d) PXRD pattern after heating **1** at 170°C for 3 h. Peaks are assigned to *hkl* index numbers of γ-CuI nanocrystals.

specimens of **1** and **2** at 105°C, which are composed of an unidentified pattern (identified as the cubane Cu<sub>4</sub>I<sub>4</sub> polymer **3**, marked with open circles in Figure 1; Figures S10, S11 and Tables S7, S8 in the Supporting Information) and a pattern assigned to the  $\gamma$ -CuI nanocrystals (marshite syn., JCPDS 00-006-0246, marked with asterisk in Figure 1). This is not surprising since both coordination polymers are composed of the same 2D layer structure unit as mentioned above. Observed PXRD patterns of **1** and **2** are matched with PXRD patterns calculated from the SCXRD data as shown in Figure 1 and Figure S10 in the Supporting Information, respectively. Both heated samples show the same photoluminescence spectra with  $\lambda_{\text{max}} = 528$  nm when they were irradiated by UV light, which originated from the compound **3** (Figure S12 in the Supporting Information). Photoluminescence is a characteristic property of the cubane Cu<sub>4</sub>I<sub>4</sub> cluster.<sup>[16,17]</sup> Good-quality crystals of **3** were formed when **2** was heated at 150°C for 48 h. The crystal structure of **3** by SCXRD analysis shows a 1D loop-chain coordination polymer with inner metallomacrocycles based on cubane Cu<sub>4</sub>I<sub>4</sub> clusters, which is topologically the same as tubular 1D coordination polymers (Scheme 1 and Figure S11 in the Supporting Information).<sup>[18,19]</sup> The observed PXRD pattern of **3** is matched with the PXRD pattern calculated from the SCXRD data as shown in Figure S13 in the Supporting Information.

Transmission electron microscopy (TEM) images after heating **2** at 170°C for 1, 6, and 24 h show nanoparticles with approximate sizes of 20, 30, and 50 nm, respectively (Figure 2). The particle sizes were also confirmed from TEM images in agreement with the values calculated from PXRD using the Scherrer equation (Figures S14, S15 and Tables S9, S10 in the Supporting Information). The coordination polymer **1** is transformed into  $\gamma$ -CuI nanocrystals faster than **2** (Figures S14 and S15 in the Supporting Information). The growth rate difference comes from the difference in CuI content in **1** and **2**. At an early stage of the reaction, round-shaped  $\gamma$ -CuI particles with average size of 20 nm are readily observable (Figure 2a); the several small particles then aggregate to form larger particles (Figure 2c) and ultimately form hexagonal and truncated triangular-shaped nanocrystals as large as 50 nm (Figure 2d). These observations suggest that the crystal growth proceeds through an Ostwald ripening mechanism. The high-resolution TEM image shown in Figure 2e is also in agreement with the growth mechanism because most atomic arrays in the crystal are the same except for a small part indicated by a white circle. All TEM images in Figure 2b show visible lattice fringes (Figure S16 in the Supporting Information), which indicate their single-crystalline nature. Fourier transform of the TEM image shown in Figure 2f gives nice hexagonal spots which correspond to the (111) plane of  $\gamma$ -CuI and indicate that the nanoparticle is single-crystalline. The  $d$  spacing of 3.49 Å corresponds to the (111) plane of  $\gamma$ -CuI (Figure S16b in the Supporting Information). Chemical compositions of the particles were determined by energy-dispersive X-ray (EDX) spectroscopy before and after heat-

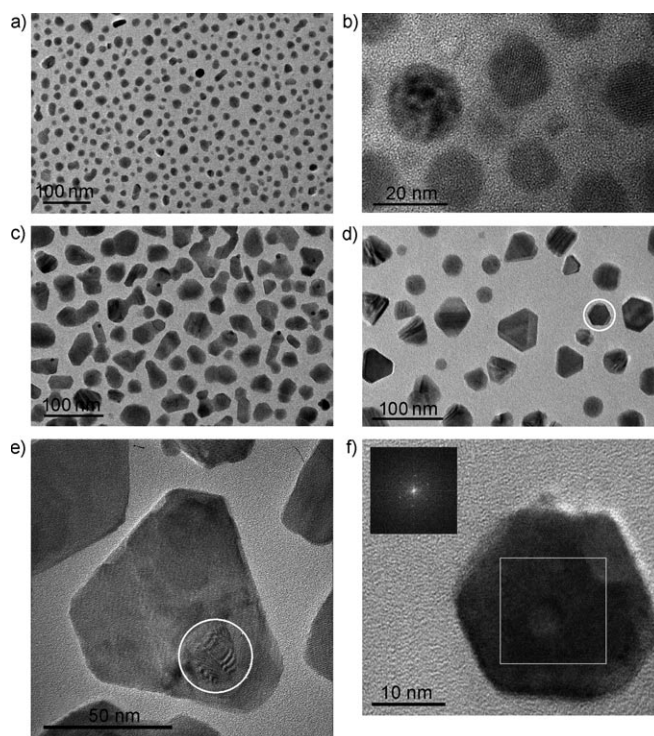


Figure 2. TEM images of  $\gamma$ -CuI nanocrystals. a) TEM image of  $\gamma$ -CuI nanocrystals from heating **2** at 170°C for 1 h. b) Enlarged image of a. c) TEM image of  $\gamma$ -CuI nanocrystals from heating **2** at 170°C for 6 h. d) TEM image of  $\gamma$ -CuI nanocrystals from heating **2** at 170°C for 24 h. e) High-resolution TEM image of  $\gamma$ -CuI crystals. f) Enlarged TEM image of a  $\gamma$ -CuI nanocrystal marked with a white circle in d. Inset is a Fourier transform of the image marked with a white square (111).

ing (Figures S17, S18 and Tables S11, S12 in the Supporting Information). In addition to peaks corresponding to Cu and I, the sulfur peak at 2.3 keV is strong for the coordination polymers before heating, while a trace peak of S is observed for  $\gamma$ -CuI nanocrystals after heating (Tables S11 and S12 in the Supporting Information).

Synthetic conditions of two self-assembled copper(I) coordination polymers, **1** and **2**, have been controlled by the mole ratio of reactants and solvent composition. The intermediate coordination polymer **3** was obtained by crystal transformation of **1** and **2** with heat. The copper(I) coordination polymers have been used as precursors to prepare  $\gamma$ -CuI nanocrystals for the first time. The advantages of  $\gamma$ -CuI nanocrystal preparation by this method are energy saving owing to the low-temperature preparation and environmentally friendly chemistry since the ligand can be recycled. As  $\gamma$ -CuI nanocrystals can be prepared in various sizes, this semiconducting material may find use in catalysis and the electronics industry.<sup>[20,21]</sup> Clearly, exciting opportunities remain in preparation of other nanocrystals from coordination polymer precursors with appropriate labile ligands at certain temperatures.

## Experimental Section

The  $^1\text{H}$  and  $^{13}\text{C}$  NMR spectra were recorded with a Bruker Advance-300 (300 MHz) NMR spectrometer. The FTIR spectra of the coordination polymers and ligand were measured with a Bruker Optics VERTEX 80v spectrometer. The elemental analysis was carried out on a CE EA1110 elemental analyzer. Thermogravimetric analysis (TGA) and differential thermal analysis (DTA) were performed under  $\text{N}_2(\text{g})$  at a scan rate of  $10^\circ\text{C min}^{-1}$  using a TA SDT Q600 thermal analyzer. Steady-state luminescence spectra were acquired with a Perkin–Elmer LS 50B spectrophotometer. The excitation and emission spectra were corrected for the wavelength-dependent lamp intensity and detector response, respectively. The pulsed excitation source was generated using the 330 nm of the Xenon lamp. For field-emission scanning electron microscope (FE-SEM) a piece of the compound was placed on a carbon tape after platinum coating; the specimen was then examined with a Jeol JSM-6701F. TEM images were obtained with a JEOL JEM-2010 and a FEI Tecnai F20 transmission electron microscope operation at 200 kV. Powder X-ray diffraction (PXRD) patterns were obtained with a Bruker AXS D8 DISCOVER diffractometer using  $\text{Cu}_{\text{K}\alpha}$  (1.54056 Å) radiation. The conductivity was measured by using a standard four-probe method. Single-crystal X-ray diffraction (SCXRD) data at low temperature were collected on Bruker SMART CCD (for **1** and **2**) and Bruker Ultra APEX II (for **L** and **3**) diffractometers equipped with graphite-monochromated  $\text{Mo}_{\text{K}\alpha}$  radiation ( $\lambda = 0.71073$  Å). The cell parameters for the compounds were obtained from a least-squares refinement of the spot using the SMART and APEX II programs. The intensity data were processed using the Saint Plus program. All of the calculations for the structure determination were carried out using the SHELXTL package.<sup>[22]</sup> Absorption corrections were applied by using SADABS multiscan method.<sup>[23]</sup> In most cases, hydrogen positions were input and refined in a riding manner along with the attached carbon atoms. CCDC 739725, CCDC 739726, CCDC 739727, and CCDC 739728 contain the supplementary crystallographic data for this paper. These data can be obtained free of charge from The Cambridge Crystallographic Data Centre via [www.ccdc.cam.ac.uk/data\\_request/cif](http://www.ccdc.cam.ac.uk/data_request/cif)

## Acknowledgements

The Korea Science and Engineering Foundation (KOSEF No. 2009-0074237) is acknowledged by T.H.K for support.

**Keywords:** coordination polymers • copper • crystal growth • marshallite • nanostructures

- [1] A. P. Alivisatos, *J. Phys. Chem.* **1996**, *100*, 13226–13239.
- [2] A. P. Alivisatos, *Science* **1996**, *271*, 933–937.
- [3] T. Wang, X. Hu, S. Dong, *J. Phys. Chem. B* **2006**, *110*, 16930–16936.
- [4] R. Heitz, S. Rodt, A. Schliwa, D. Bimberg, *Phys. Status Solidi B* **2003**, *238*, 273–280.
- [5] X. Liu, *Angew. Chem.* **2009**, *121*, 3062–3065; *Angew. Chem. Int. Ed.* **2009**, *48*, 3018–3021.
- [6] M. Nagarathinam, J. Chen, J. J. Vittal, *Cryst. Growth Des.* **2009**, *9*, 2457–2463.
- [7] X. Lu, M. S. Yavuz, H.-Y. Tuan, B. A. Korgel, Y. Xia, *J. Am. Chem. Soc.* **2008**, *130*, 8900–8901.
- [8] K. Tennakone, G. R. R. A. Kumara, I. R. M. Kottegoda, V. P. S. Perera, G. M. L. P. Aponsu, K. G. U. Wijayantha, *Solar Energy Materials and Solar Cells* **1998**, *55*, 283–289.
- [9] P. M. Sirimanne, M. Rusop, T. Shirata, T. Soga, T. Jimbo, *Chem. Phys. Lett.* **2002**, *366*, 485–489.
- [10] D. Kim, M. Nakayama, O. Kojima, I. Tanaka, H. Ichida, T. Nakanishi, H. Nishimura, *Phys. Rev. B* **1999**, *60*, 13879–13884.
- [11] L. P. Zhang, F. Guo, X. Z. Liu, *Mater. Res. Bull.* **2006**, *41*, 905–908.
- [12] Y. Liu, J. Zhan, J. Zeng, Y. Qian, K. Tang, W. Yu, *J. Mater. Sci. Lett.* **2001**, *20*, 1865–1867.
- [13] A. Chahid, R. L. McGreevy, *Physica B* **1997**, *234–236*, 87–88.
- [14] W. Sekkal, A. Zaoui, *Physica B* **2002**, *315*, 201–209.
- [15] M. Protiva, J. Pliml, P. Finglova, *Chemické Listy pro Vedu a Prumysl* **1953**, *47*, 1197–1203.
- [16] T. H. Kim, Y. W. Shin, J. H. Jung, J. S. Kim, J. Kim, *Angew. Chem.* **2008**, *120*, 697–700; *Angew. Chem. Int. Ed.* **2008**, *47*, 685–688.
- [17] P. C. Ford, E. Cariati, J. Bourassa, *Chem. Rev.* **1999**, *99*, 3625–3647.
- [18] A. J. Blake, N. R. Brooks, N. R. Champness, M. Crew, D. H. Gregory, P. Hubberstey, M. Schröder, A. Deveson, D. Fenske, L. R. Hanton, *Chem. Commun.* **2001**, 1432–1433.
- [19] T. H. Kim, Y. W. Shin, S. S. Lee, J. Kim, *Inorg. Chem. Commun.* **2007**, *10*, 11–14.
- [20] J. Gan, D. Ma, *Org. Lett.* **2009**, *11*, 2788–2790.
- [21] P. M. Sirimanne, *Renewable Energy* **2008**, *33*, 1424–1428.
- [22] G. M. Sheldrick, Bruker, SHELXTL-PC, Version 5.10, Bruker-Analytical X-ray Services, Madison, WI, **1998**.
- [23] G. M. Sheldrick, SADABS Software for Empirical Absorption Correction, University of Göttingen, Göttingen, Germany, **2000**.

Received: September 1, 2009  
Published online: December 26, 2009